Comparison of Experimental results with CFD for NREL Phase VI Rotor with Tip Plate

EswaraRao Anjuri VSJ*‡

*Turbine CFD, Vestas Technology R&D, Chennai, India

esran@vestas.com

‡Corresponding Author; EswaraRao Anjuri VSJ, Turbine CFD, Vestas Technology R&D, Chennai, India, esran@vestas.com

Received: 28.06.2012 Accepted: 06.08.2012

Abstract- This article presents the results of 3D CFD rotor computations of a NREL Phase VI rotor with tip plate, a stall-regulated turbine with full-span pitch control, has a power rating of 20 kW. In this paper, A full three dimensional CFD-RANS approach by modeling the whole rotor of a wind turbine by means of periodicity was used. All the simulations were performed using the commercial multi-purpose CFD solver ANSYS CFX 12.1 with the transition model of Langtry and Menter is applied to a rotor at stationary wind conditions without wind shear. The comparisons were done for the blade with 0° yaw angle and 3° tip pitch angle on a single rotor blade without tower and nacelle. Reasonably good agreement is obtained when comparing modeled mechanical effects like power and thrust with findings from measurements. Similarly the spanwise force distributions are compared with experimental results for two wind speeds along with pressure distributions at five different spanwise locations. It is shown capability of 3D CFD computations that can be used to extract information about three-dimensional aerodynamic effects.

Keywords- Navier–Stokes, Computational fluid dynamics, Wind turbine aerodynamics, NREL Phase VI Rotor, Tip Plate.

1. Introduction

Accurate aerodynamic predictions are very much required in the design of new rotor blades and additional features that improve performance. This requires continued validation of new and existing design tools (ex. CFD), increased accuracy and efficiency of the results. Extensive research has been done in developing the CFD tools and methods for predicting aerodynamic flows of wind turbines during the last few years.

During the last decade, CFD modelling of wind turbines have evolved from scientific work performed at research institutions with the application of commercial codes. However, BEM models are dependent on empirical corrections to 2D airfoil tables to account for 3D effects, such as tip loss, rotational flow, and dynamic stall. High fidelity CFD naturally includes these phenomena, but has more difficulty in modelling other wind turbine phenomena such as variable turbulent inflow and boundary layer transition [8]. CFD has been used to improve the aerodynamic design of wind turbines including tip shapes, winglets and hub modelling [9-12] where it captures flow physics better at which BEM models are no longer applicable. High fidelity Navier-Stokes computational fluid dynamics is currently making inroads into many phases of industrial wind energy design [1, 2]. CFD is used for the analysis of both 2D airfoils and also 3D blades [1, 3-6].

The objective of the present work is to validate the CFD results at two different wind speeds using commercial multi-purpose CFD solver ANSYS CFX 12.1, on the NREL Phase VI rotor with tip plate (Test sequence V) wind turbine dataset. The NREL Phase VI Unsteady Aerodynamic Experiment [1, 2, 18] provides an excellent validation test case for CFD analyses. The Phase VI test campaign performed in the NASA Ames National Full-Scale Aerodynamic Complex (NFAC) was completed in the year 2000. The 2-bladed, 10.058m diameter, stall regulated turbine has a power rating of 20kW. The blades are twisted and mildly tapered. Multidisciplinary measurements were obtained over a wide range of operating conditions. Experimental measurements included blade pressures and resulting integrated air loads, shaft torque, sectional inflow conditions, blade root strain, tip acceleration and wake visualization. Both upwind and downwind configurations

with rigid and teetering blades were run for speeds from 5 to 25m/s. Yawed and unsteady pitch configurations are also available. Free and fixed transition results were measured. The blade uses specially designed S809 airfoils for which experimental aerodynamic performance parameters are available. Various researchers [2, 3, 8, 13, 14, 16-20] have investigated this configuration numerically using a range of CFD methods and grid topologies.

Researchers at Risø computed the isolated rotor with and without wind tunnel walls using a multi-block, structured mesh, incompressible solver EllipSys3D with a RANS turbulence model [20] and a detached eddy simulation [8]. Performance was generally well captured although stall initiation at 10m/s wind speed was missed. Zahle at Risø used the overset, structured mesh incompressible solver EllipSys3D to model the rotor and tower configurations [19].

A lot of research work has been performed on NREL Phase VI rotor without any additional attachments to the blades and compared the CFD results with experimental data (as mentioned above). The present work focuses on NREL Phase VI Rotor with Tip Plate (Sequence V of experimental configuration) and compares the CFD results with experimental data.

The scientific contributions of the paper are:

- Modelling of Tip Plate on the NREL Phase VI Rotor.
- Analysing the configuration at two different wind velocities and compare power and thrust results.
- Compare pressure distribution and normal force coefficient results with experimental data.
- Analyse the flow behaviour on rotor blade with the help of surface streamlines.
- Demonstrate the capabilities of CFD in predicting the behaviour of non-planar rotors.

The remainder of the paper was organized as follows: Section 2 explains the modelling and meshing of the NREL Phase VI rotor using ANSYS CFX, boundary conditions and computational time. Section 3 explains the details of NREL Phase VI rotor. Section 4 describes the results from CFD and comparison with experimental data and finally Section 5 gives the summary of the findings and relevant conclusions of the present work.

2. Methodology

2.1. Navier–Stokes Solver (CFX)

In the present work a compressible Navier-Stokes solver (CFX) is applied to predict the aerodynamics of the Phase VI rotor with tip plate from the National Renewable Energy Laboratory. The two-bladed 10.058m diameter (9.886 m with tip plate, Sequence V) rotor geometry is based on the S809 airfoil, and details about the blades can be found in [7]. The rotor cone angle was set at 0^o and the pitch angle was set at 3^o. (Rotated the blade tip chord line 3^o towards feather relative to the rotor plane, pointing the leading edge into the oncoming wind). In this investigation, only the upwind configuration was examined, and the operational conditions for the cases computed can be found in Table I.

Table 1. Operating conditions

Wind Speed (m/s)	Yaw (deg)	Rotational Speed (RPM)	Density (kg/m^3)
7.057552	0.001343	71.840805	1.233689
8.062965	0.001343	71.956619	1.233805

In the current work, only one of the blades is modelled for CFD computations considering the periodic boundary conditions of 180^o of the rotor in order to save computational resources. Only the wind speed, RPM and density values are needed for CFD simulations as there is no empirical tuning is required.

All computations have been performed with the commercial general purpose CFD codes, ANSYS CFX 12.1. It uses a finite-volume based unstructured parallelized coupled algebraic multi grid solver with a second order advection scheme and second order overall accuracy. The computations have been performed with the compressible version of the Reynolds Averaged Navier-Stokes (RANS) equations and the SST [15] turbulence models. The rotor computations have primarily been performed with Langtry and Menter correlation based transition model [4]. The default correlations in the model are proprietary by ANSYS and therefore not known in detail by the user. In general the default correlation for momentum thickness Reynolds number ($R_{e\theta t}$) is based on the free stream turbulence intensity and the pressure gradient outside the boundary layer. The value of $R_{e\theta t}$ determined outside of the boundary layer is diffused into the boundary layer by a standard diffusion term. The physics of the transition process is not directly modelled by the two additional transport equations. Instead, the physics of the transition process is entirely contained in the underlying experimental correlations. All computations have been run in parallel on the in-house computing cluster at Vestas Technology R&D Center, India.

2.2. Rotor Modelling and Meshing

Only one blade was modelled with 1800 periodicity to save the computational resources. The use of periodicity prevents the possibility to include wind shear or yaw errors in the model. As the turbine is upwind type, tower was not included in the simulation assuming the negligible effect of tower on rotor aerodynamics. Rotor computations are stationary, performed at constant uniform wind speeds neglecting the unsteady inflow and constant pitch and RPM. The computations are performed with transition model so that boundary layer is modelled with free transition.

A block structured hexahedral mesh is applied for the main part of the mesh and a y+ smaller than approximately two is utilized for most of the blade in order to ensure a well resolved boundary layer and fulfillment of the SST turbulence model criteria. A H-mesh is applied, since this fits well for the outermost part of the blade. In the spanwise direction 128 grid points are located along the blade, and a

resolution of 227 grid points are applied in the chord-wise direction with an expansion ratio of 1.1 in the directions away from the blade with total mesh nodes of 14.6 million. The computational mesh extends five rotor radii upstream, eight rotor radii downstream of the turbine and five rotor radii in the radial directions (i.e., in the blade span-wise direction) to ensure that the flow at the turbine is unaffected by the presence of the outer boundaries.

2.3. Boundary Conditions used for CFD simulation

Uniform velocity normal to the boundary is used as inlet boundary condition and static pressure is used as boundary condition for outlet and far-field surfaces. Blade and hub surfaces are defined as no slip walls with rotation. In the present work the turbulence in the boundary layer is modelled by k-ω SST with Gamma-Theta Transition model. Figure 1 shows the different boundaries including the blade with tip plate and Figure 2 shows the mesh on the different boundaries including the blade with tip plate.

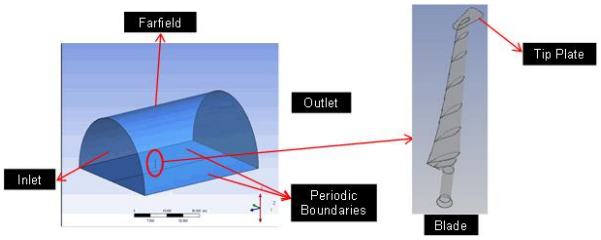

Fig. 1. Computational domain and blade with Tip Plate

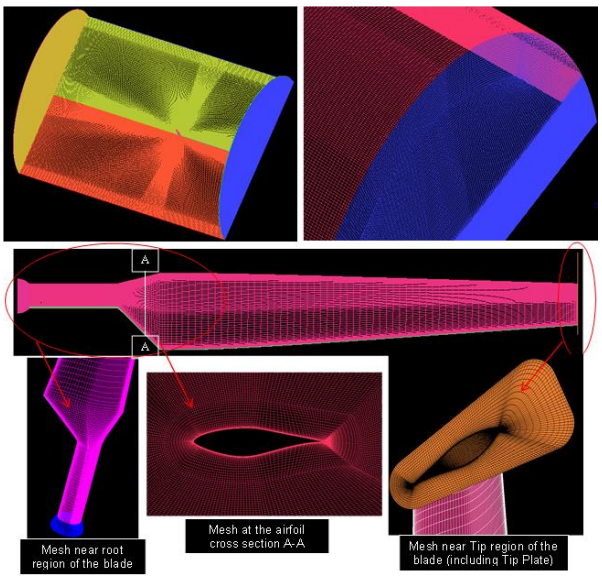

Fig. 2. Computational mesh in the domain and blade with Tip Plate

2.4. Computing Time

All computations have been run in parallel on the in-house computing cluster at Vestas Technology R&D Center, India. The steady state simulations were performed for 1000 iterations making sure that required convergence is achieved.

3. NREL Phase VI Rotor Configuration

The NREL Phase VI rotor geometry, aerodynamic and structural properties are well-documented in the literature [7]. The theoretical definition of the S809 airfoil has a very sharp trailing edge. Whereas the geometry used for CFD simulations was modified so that the trailing edge thickness was 1mm all along the blade which may introduces some discontinuities in the results. In the geometry modelling the spherical hub has been extended to connect the two blades. The upwind configuration "Sequence V" has been used for the present study and comparison. The operating condition for the experiment was varied from wind speed of 7 to 25 m/s. The rotor RPM is 72, with the tip pitch is 3 degree and zero cone angle. The rotor radius is 4.943m with tip plate.

4. Results and Discussion

Mechanical Power (P) is calculated by monitoring the torque (T) about the flow axis and multiplying with the angular velocity (Ω) (as shown in equation 1).

$$P = T\Omega \quad (1)$$

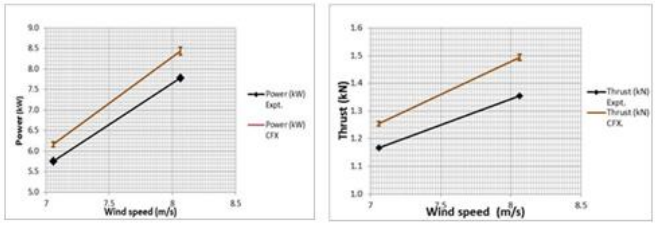

Fig. 3. Comparison of CFD and measured power and thrust

It is observed that power and thrust are over-predicted with CFD at both wind velocities. In the following, the spanwise distribution of normal force coefficient is compared with measurements, followed by a comparison of computed and measured pressure distributions.

Reasonably good agreement is observed in the comparison of spanwise distribution of the normal force coefficient with experimental results (as shown in Figure 4).

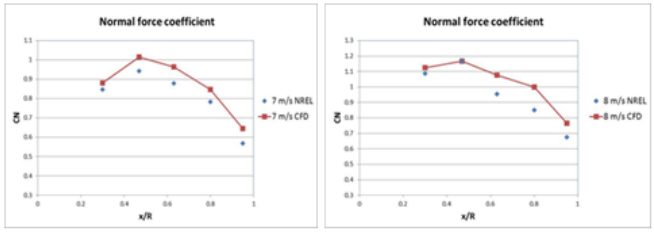

Fig. 4. Comparison of CFD and measured normal force coefficient at 7m/s and 8m/s

Even though quantitative differences exist in the normal force coefficient, the trends of the computed CN curve agree well with the measured curve for both wind velocities. Accuracy of the turbulence models may be one of the reasons for the deviation of CFD results with experimental results.

4.1. Pressure Distributions

Surface pressure distributions are shown in Figure 5 and Figure 6 for 7 m/s and 8 m/s wind velocities. In the experimental data, the stagnation point dynamic pressure is used for non-dimensionalisation. The calculations use a dynamic pressure based on a combination of the wind speed and local rotor section speed, $0.5\rho\,[v^2 + (r\omega)^2]$. Pressure distributions at 7 m/s and 8 m/s wind velocities are in good agreement with the test data.

In the following, comparisons of measured and computed pressure distributions will be shown. In the experiment, pressure distributions for five spanwise sections are measured at r/R 30%, 46.7%, 63.3%, 80% and 95%. Figure 5 shows comparison of Cp at 7m/s wind speed.

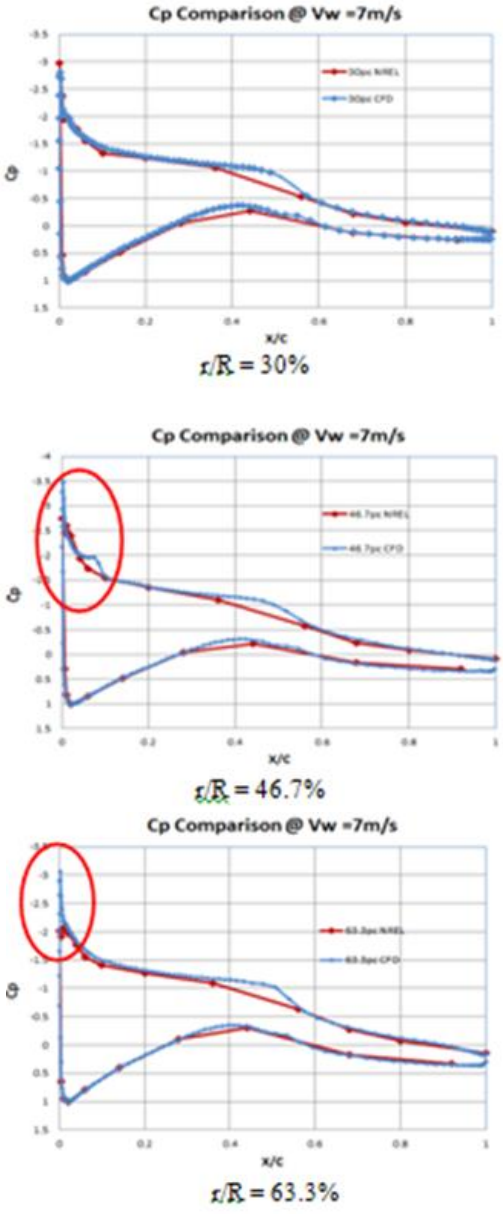

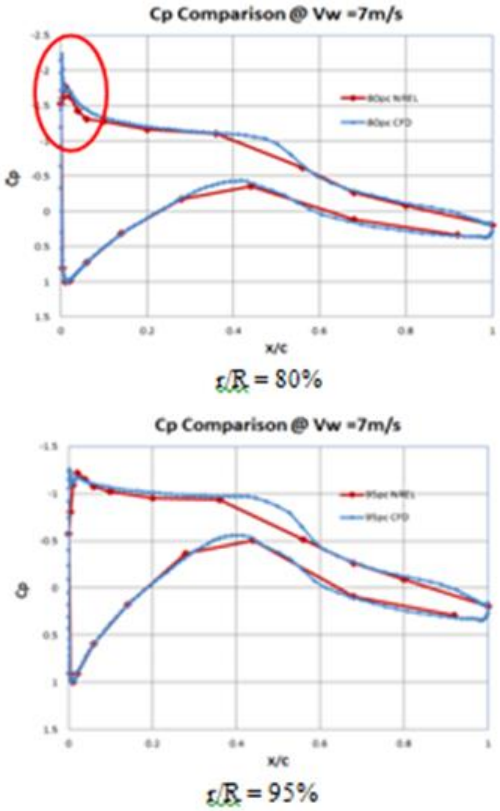

Fig. 5. Comparison of CFD and measured pressure distribution

The flow is mostly attached at the outboard station and is in good agreement with the measured data. Pressure predictions are generally good at all the spanwise locations, with some discrepancy in the pressure level and the near the leading edge of the suction surface of the blade. Figure 6 shows comparison of Cp at 8m/s wind speed.

The pressure distributions match well at 8m/s wind speed flow is mostly attached at the outboard station and is in good agreement with the measured data. Pressure predictions are generally good at all the spanwise locations, with some discrepancy in the pressure level and the near the leading edge of the suction surface of the blade.

Below figure (Figure 7) shows the comparison of difference in pressure distribution from measurements to CFD at 7m/s and 8m/s wind speeds. Here the legend NREL_TP_7m/s represents the NREL Tip Plate case at 7m/s wind speed.

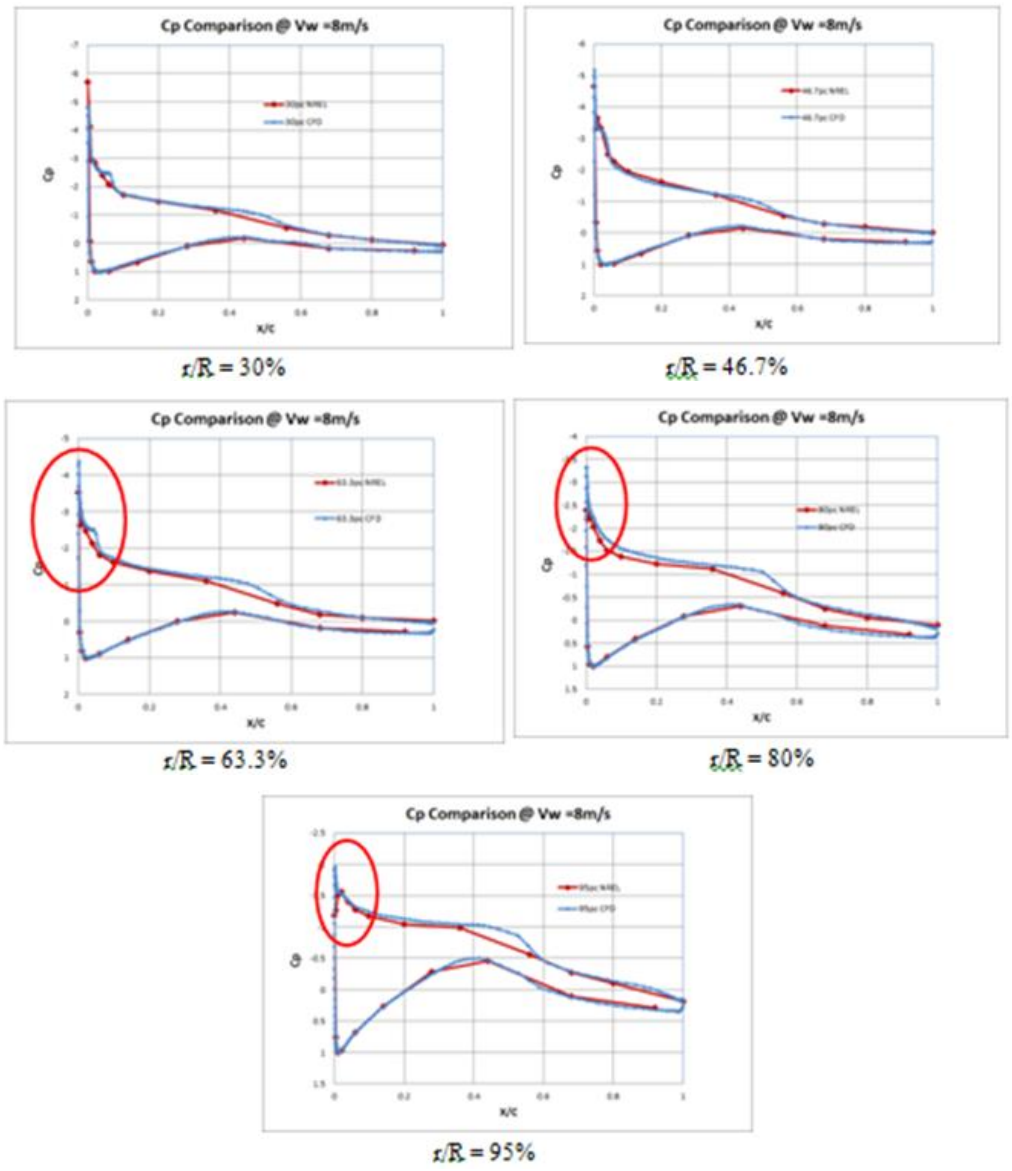

Fig. 6. Comparison of CFD and measured pressure distributions at different span wise locations for wind velocity 8m/s

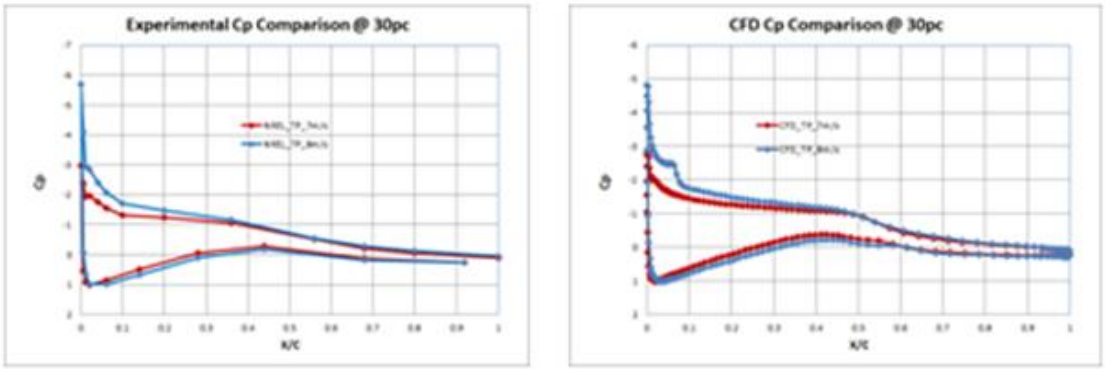

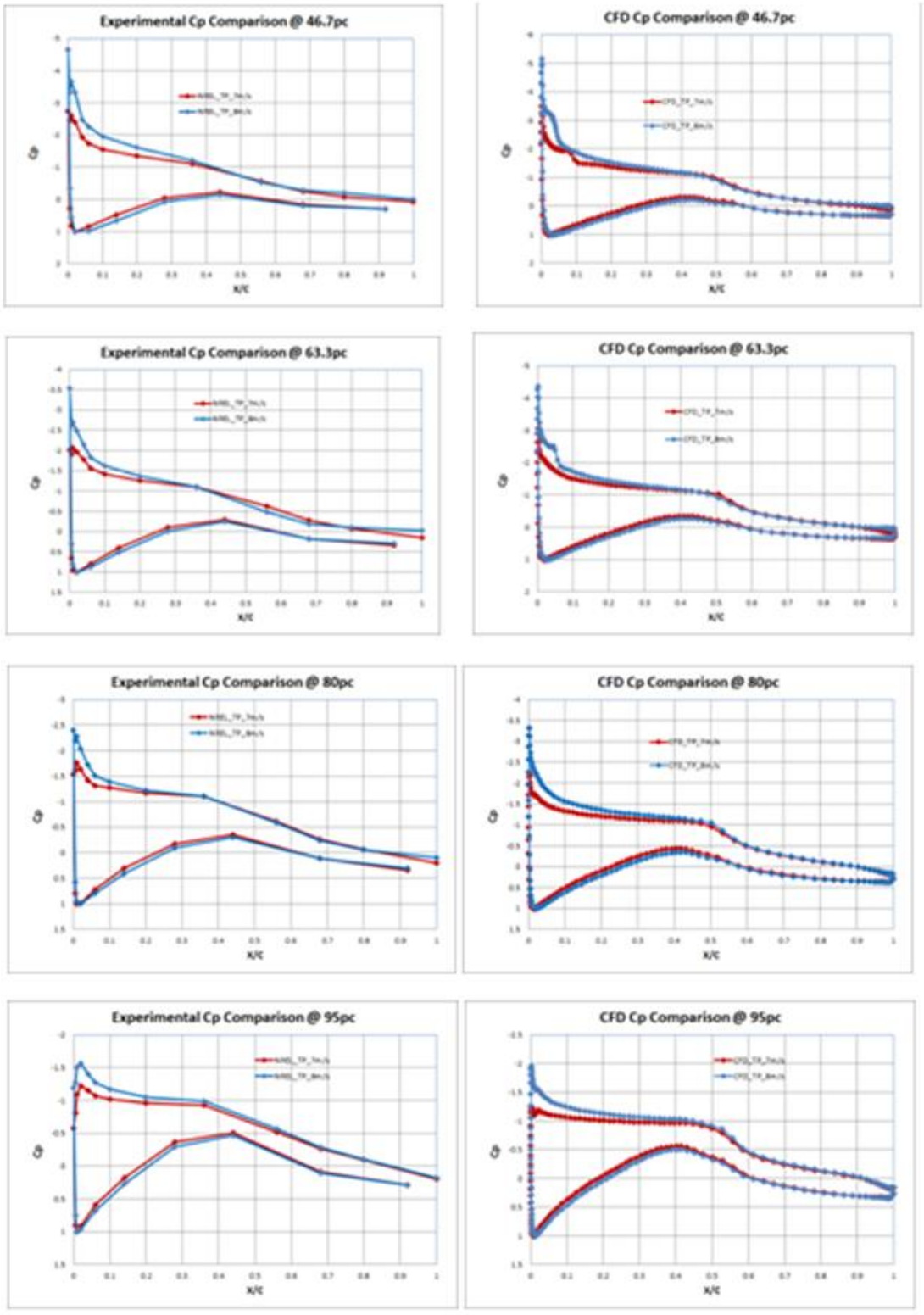

Fig. 7. Comparison of measured and CFD pressure distributions at different spanwise locations

From the above figure, it is observed that the effect of change in wind speed is similar in both measurements and CFD for all the spanwise sections. Whereas the absolute value of Cp is different in CFD when compared to experiments. CFD predicts high suction pressure in the outboard region of the blade compared to experiment. This difference may be due to low resolution of pressure taps along the chord in the test case.

4.2. Surface and Flow Field Streamlines

In order to understand the flow pattern on blade surface streamlines (oil flow) are shown below for 7m/s and 8m/s wind velocities. Below Figure 8 and Figure 9 show the streamline pattern on blade surface at 7m/s and 8m/s respectively.

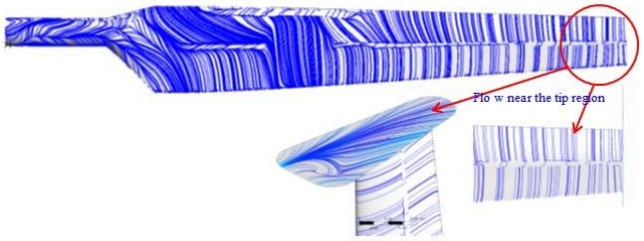

Fig. 8. Surface streamlines at 7m/s

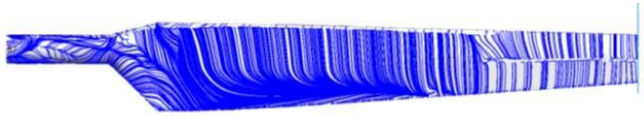

Fig. 9. Surface streamlines at 8m/s

Strong radial flow can be observed at 8m/s wind speed in the mid board region of the blade apart from radial flow very close to cylindrical region. However, as seen from the surface streamlines in Figure 8, the flow on the tip region is extremely complicated and dominated by three-dimensional effects. The dividing line from the streamlines indicates the transition location that means location of changing the flow from laminar to turbulent region. The same can be observed from the turbulence intermittency contours below as shown in Figure 10.

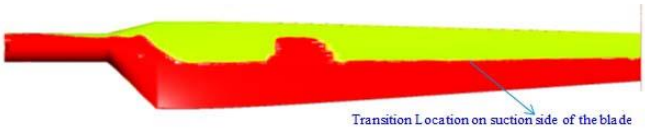

Fig. 10. Turbulence intermittency contour on suction side of the blade at 7m/s

5. Conclusion

Computational fluid dynamics calculations have been performed on the NREL Phase VI rotor with tip plate. A single blade has been analysed with 1800 periodicity and used structured mesh with commercial multi-purpose CFD solver ANSYS CFX 12.1. The CFD data is compared against the measured wind tunnel data and following conclusions were made:

1. It is shown that the 3D CFD computations can be used to determine the 3D aerodynamic effects present on wind turbine rotors.
2. Predictions using SST transitional turbulence model of CFX for NREL Phase VI rotor with tip plate differ of the order of 8.5% for power and 10.8% for thrust at 8m/s wind velocity.
3. The trends of the computed CN curve agree well with the measured curve for both wind velocities. But, the absolute values in CN show differences with experimental data.
4. The pressure distributions match well with experimental data.
5. The effect of wind speed on pressure distribution is well captured with CFD and similar differences are observed with CFD when compared to experimental data.

Acknowledgements

The author would like to thank Mr Ronald Grife, Conceptual Aero Design Engineer of Aero Systems-Vestas, USA for providing the measured data available from NASA-Ames wind tunnel. The author also wanted to thank Vestas Technology R&D Chennai Pvt. Ltd., for providing necessary computational resources and continuous support without which this study could not have performed.

References

[1] Larsen, J., "ANSYS CFD Applied to Wind Turbines at Siemens Wind Power," ANSYS Conference & 26th CADFEM Users' Meeting, Darmstadt, Germany, October 2008.

[2] Mark A. Potsdam, Dimitri J. Mavriplis, "Unstructured Mesh CFD Aerodynamic Analysis of the NREL Phase VI Rotor", AIAA 2009-1221, 47th AIAA Aerospace Sciences Meeting Including The New Horizons Forum and Aerospace Exposition, 5 - 8 January 2009, Orlando, Florida.

[3] Le Pape, A., and Gleize, V., "Improved Navier-Stokes Computations of a Stall-Regulated Wind Turbine Using Low Mach Number Preconditioning," 44th AIAA Aerospace Sciences Meeting and Exhibit, Reno, NV, January 2006, AIAA 2006-1502.

[4] Robin Langtry, Florian Menter, "Overview of Industrial Transition Modelling in CFX", ANSYS Germany GmbH, ANSYS CFX.

[5] Standish, K. J., and van Dam, C. P., "Aerodynamic Analysis of Blunt Trailing Edge Airfoils," Journal of Solar Energy Engineering ,Vol. 125, No. 4, Nov. 2003, pp. 479-487.

[6] Fuglsang, P., and Bak, C., "Development of the Risø Wind Turbine Airfoils," Wind Energy, Vol. 7. No. 2, May 2004, p. 145-162.

[7] M.M. Hand, D.A. Simms, L.J. Fingersh, D.W. Jager, J.R. Cotrell, S. Schreck, and S.M. Larwood, "Unsteady Aerodynamics Experiment Phase VI: Wind Tunnel Test Configurations and Available Data Campaigns", NREL/TP-500-29955, December 2001.

[8] Johansen, J., Sørensen, N. N., Michelsen, J. A., and Schreck, S., "Detached-Eddy Simulation of Flow around the NREL Phase-VI Rotor," Wind Energy, Vol. 5, No. 2-3, 2002, pp. 185-197.

[9] Johansen J., Madsen, H. A., Sørensen, N. N., and Bak C., "Numerical Investigation of a Wind Turbine Rotor with an Aerodynamically Redesigned Hub-Region," 2006 European Wind Energy Conference and Exhibition, Athens, Greece, 2006.

[10] Johansen J., and Sørensen N. N.: "Aerodynamic investigation of winglets on wind turbine blades using CFD", Risø-R- 1543(EN) report 2006.

[11] Hansen, M. O. L., and Johansen, J., "Tip Studies Using CFD and Comparison with Tip Loss Models," Wind Energy, 2004, p. 343 -356.

[12] Hjort, S., Laursen, J., and Enevoldsen, P., "Aerodynamic Winglet Optimization," Sandia National Lab Blade Workshop, May 2008.

[13] Duque, E. P. N., Burklund, M. D., and Johnson, W., "Navier-Stokes and comprehensive analysis performance predictions of the NREL phase VI experiment," Journal of Solar Energy Engineering 2003; 125: 457-467.

[14] Chao, D. D., Van Dam, C. P., "Computational Aerodynamic Analysis of a Blunt Trailing-edge Airfoil Modification to the NREL Phase VI Rotor," Wind Energy, July 2007, 10:529-550.

[15] Menter FR. "Two-equation eddy-viscosity model for engineering applications". AIAA-Journal 1994; 32(8):1598-1605.

[16] Gonzalez A., Munduate, X., "Three-dimensional and Rotational Aerodynamics on the NREL Phase VI Wind Turbine Blade," 45th AIAA Aerospace Sciences Meeting and Exhibit, Reno, NV, January 2007, AIAA 2007-0628.

[17] Schmitz, S., Chattot, J-J., "Application of a 'Parallelized Coupled Navier-Stokes/Vortex Panel Solver' to the NREL Phase VI Rotor," 43rd AIAA Aerospace Sciences Meeting and Exhibit, Reno, NV, January 2003, AIAA 2003-0593.

[18] Zahle, F., Johansen, J., Sorenson, N., and Graham, J., "Wind Turbine Rotor-Tower Interaction Using an Incompressible Overset Grid Method," AIAA 45th Aerospace Sciences Meeting and Exhibit, Reno, NV, January 2007, AIAA 2007-0425.

[19] Simms, D. A., Schreck, S., Hand, M., and Fingersh, L., J., "NREL Unsteady Aerodynamics Experiment in the NASA Ames Wind Tunnel: A Comparison of Predictions to Measurements" NREL/TP-500-29494, June 2001.

[20] Sørensen, N. N., Michelsen, J. A., and Schreck, S., "Navier-Stokes Predictions of the NREL Phase VI rotor in the NASA Ames 80ft x120ft wind tunnel," Wind Energy, Vol. 5, No. 2-3, 2002, pp. 151-169.

Nomenclature

P = Rotor Mechanical Power (W)
T = Rotor Torque (N-m)
CN = Normal force coefficient
Ω = Angular Velocity (rad/s)
Cp = Pressure coefficient
r = Radial position from hub (m)
R = Rotor radius (m)
x = Chordwise position (m)
c = Rotor chord (m)
ρ = Density (kg/m^3)
v = Wind velocity (m/s)
ω = RPM
y^+ = Non-dimensional distance of the first grid point off the blade surface